Hindawi
Journal of Nanomaterials
Volume 2019, Article ID 7458645, 8 pages
https://doi.org/10.1155/2019/7458645

Research Article

Preparation of Few-Layered WS_2 and Its Thermal Catalysis for Dihydroxylammonium-5,5′-Bistetrazole-1,1′-Diolate

Yiping Shang,[1] **Wu Yang**,[1] **Yabei Xu**,[1] **Siru Pan**,[2] **Huayu Wang**,[1] **and Xiong Cao**[1]

[1]*School of Environment and Safety Engineering, North University of China, Taiyuan, Shanxi Province 030051, China*
[2]*Institute of Safety Technology of Ordnance Industry, Beijing 100053, China*

Correspondence should be addressed to Xiong Cao; cx92rl@163.com

Received 8 August 2019; Revised 13 October 2019; Accepted 19 October 2019; Published 6 December 2019

Academic Editor: Ashok K. Sundramoorthy

In this study, few-layered tungsten disulfide (WS_2) was prepared using a liquid phase exfoliation (LPE) method, and its thermal catalytic effects on an important kind of energetic salts, dihydroxylammonium-5,5′-bistetrazole-1,1′-diolate (TKX-50), were investigated. Few-layered WS_2 nanosheets were obtained successfully from LPE process. And the effects of the catalytic activity of the bulk and few-layered WS_2 on the thermal decomposition behavior of TKX-50 were studied by using synchronous thermal analysis (STA). Moreover, the thermal analysis data was analyzed furtherly by using the thermokinetic software AKTS. The results showed the WS_2 materials had an intrinsic thermal catalysis performance for TKX-50 thermal decomposition. With the few-layered WS_2 added, the initial decomposition temperature and activation energy (E_a) of TKX-50 had been decreased more efficiently. A possible thermal catalysis decomposition mechanism was proposed based on WS_2. Two dimensional-layered semiconductor WS_2 materials under thermal excitation can promote the primary decomposition of TKX-50 by enhancing the H-transfer progress.

1. Introduction

Dihydroxylammonium-5,5′-bistetrazole-1,1′-diolate (TKX-50) [1, 2] is a synthetic high-energy-density material which has a high detonation velocity, high density, and low toxicity properties. It is considered as one of the substitutes to conventional energetic materials (EM) [3–7], such as RDX and HMX. It is interesting and valuable to study thermal decomposition behavior and thermodynamics for its potential applications.

Transition metal dichalcogenide (TMD) materials [8, 9] have attracted much attention for diverse applications in various fields due to their unique optical and electrical properties [10, 11]. Bulk TMD materials can be exfoliated to form few-layered materials through micromechanical and electrochemical methods. During the exfoliating process, sandwiched tungsten and sulfur layers were peeled off as strong interlayer bonding and weak interlayer van der Waals interactions were broken by solvent action and ultrasound waves. As a novel few-layered material, exfoliated TMD materials show superior properties than raw TMD materials [12–15]. Its catalytic activity would significantly improve, since there would be more exposed edges, better conductivity, and more exposed area on the material's surface [16, 17]. Additionally, samples after the exfoliation process provide more surface areas and produce an abundance of surface-active sites [18].

As a typical TMD material, tungsten disulfide (WS_2) is widely used as a catalyst in photochemistry and electrochemistry fields due to its unique physical, optical, electrical, and structural properties [19–22]. However, the applications of WS_2 as a catalyzer in the energetic materials have not been reported. It is of great importance and significance to study thermal decomposition performance of TKX-50 by using WS_2 as thermal catalyst [23].

In this study, few-layered WS_2 was prepared by bulk exfoliation via the liquid phase exfoliation (LPE) method. The catalytic properties of raw and as-obtained WS_2 for TKX-50 thermal decomposition were studied through STA. Furthermore, activation energy (E_a) was calculated by using thermal kinetic software AKTS. A possible thermal catalysis mechanism of TKX-50 was provided with the WS_2 added.

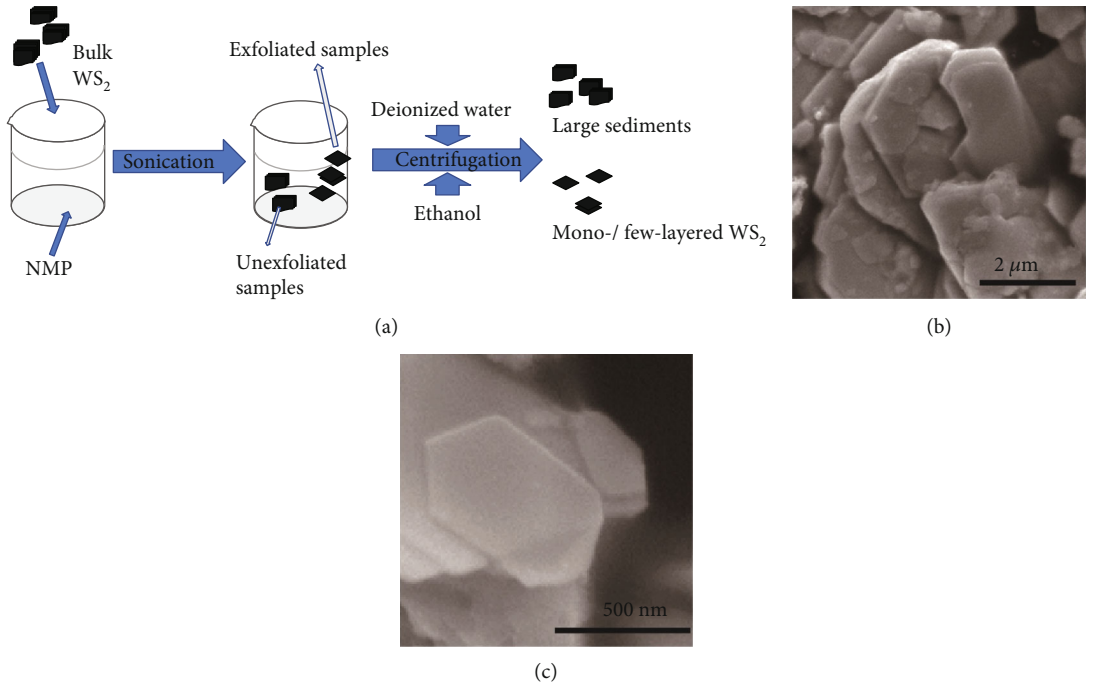

Figure 1: (a) Illustration of the exfoliate procedure of WS_2. (b) Morphology of bulk WS_2 in a scanning electron microscope (SEM) image. (c) Morphology of processed WS_2 in a SEM image.

This work offers a new way to design and fabricate TKX-50-based composite with high thermal decomposition performances.

2. Experiment

2.1. Materials. N-Methyl pyrrolidone (NMP, >99.5% (GC)) and bulk WS_2 (average 2 μm, 99.9%) were purchased from Shanghai Aladdin Bio-Chem Technology Co. Ethanol was bought from Tianjin Beilian Chemical Co. Ltd. TKX-50 was provided from the Institute of Chemical Materials, CAEP. These four chemicals were used as received without further purification. The few-layered WS_2 were prepared by the LPE method. Deionized water was homemade in the lab.

2.2. Preparation of Few-Layered WS_2. First, 20 mg of the bulk WS_2 and 30 mL of NMP were mixed together into a glass vial. The solution was then sonicated in an ultrasonic machine at a frequency of 60 kHz, until the sample became a colloidal suspension. Next, large sediments and NMP were separated in a centrifuge washed by a mixture of deionized water and ethyl alcohol in different ratios. Finally, the few-layered WS_2 was obtained in an oven after drying at 50°C. The exfoliating progress by the LPE method is shown in Figure 1(a). Bulk structure for raw WS_2 in Figure 1(b) would be exfoliated into a few-layered structure for the processed WS_2 in Figure 1(c).

2.3. Characterization and Tests. Scanning electron microscopy (SEM) and transmission electron microscopy (TEM) were performed to analyze the morphology of exfoliated WS_2 in a Libra 200 microscope (ZEISS, German) operated at 200 kV and a field emission scanning electron microscope (Tescan Mira 3 LMH Czech Tescan Company), respectively.

Table 1: Composition of samples (wt%).

Sample	B1	F1	B3	F3	Pure TKX-50
TKX-50	99	99	97	97	100
Bulk WS_2	1	—	3	—	—
Few-layered WS_2	—	1	—	3	—

For crystal structure analysis, Raman spectra were collected on a Raman spectrophotometer (DXR-smart Raman) and X-ray powder diffraction (XRD) analysis was performed on a DX_2700 X-ray diffractometer (Dandong Haoyuan Co. Ltd.).

Thermal gravity analysis (TGA) and differential scanning calorimetry (DSC) data were investigated by a simultaneous thermal analyzer (STA) 449F3 Jupiter (Germany, NETZSCH) at a temperature range of 40-400°C under condition of argon to analyze the WS_2's effects on the decomposition of TKX-50. Bulk and few-layered WS_2 was mixed with TKX-50 severally for 1 wt% and 3 wt% at different heating rates (5, 10, 15, and 20 K·min^{-1}) under 99.9% argon atmosphere. Samples were named B1, F1, B3, F3, and TKX-50 presented in Table 1 in order to represent the five samples conveniently. Kinetic analysis of thermal decomposition was carried out by a thermal analysis software AKTS (Setaram Co. Ltd. France).

3. Results and Discussions

3.1. Structural Analysis. As shown in Figure 2(a), the diffraction pattern of the bulk WS_2 has five peaks appearing at 14.35°, 39.45°, 43.95°, 49.65°, and 75.85°, corresponding to

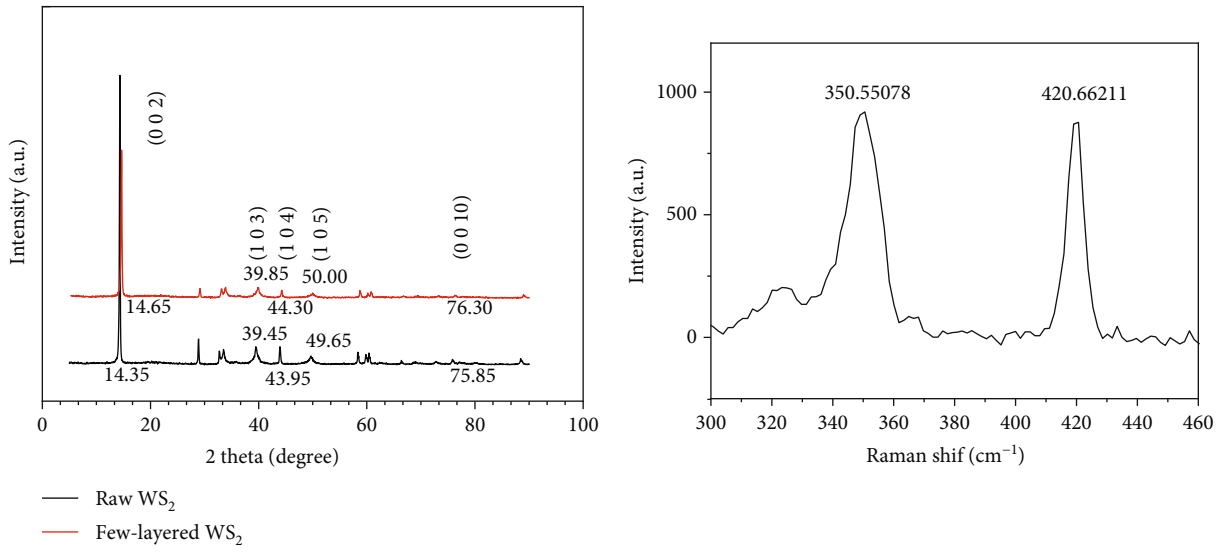

Figure 2: (a) XRD patterns of the processed and raw WS_2. (b) Raman spectra of the processed WS_2.

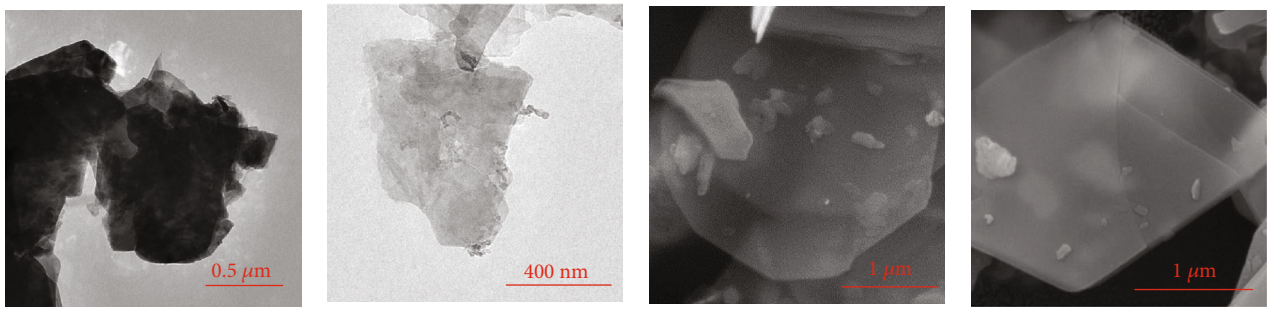

Figure 3: (a) TEM image of bulk WS_2. (b) TEM image of treated WS_2. (c, d) SEM images of the processed sample.

(0 0 2), (1 0 3), (1 0 4), (1 0 5), and (0 0 10) of 2H-phase WS_2 (JCPDS 04-003-5636). The XRD pattern of the processed WS_2 was consistent with the bulk one indicating that each of the two WS_2 was in the 2H phase. Raman modes located at 350 and 420 cm^{-1} in Figure 2(b) further confirmed that the processed WS_2 had all the characteristics of the 2H phase WS_2, which was consistent with the XRD results.

3.2. Morphological Analysis. Morphological results were analyzed from the TEM and SEM images. The TEM image of bulk and treated WS_2 shown in Figures 3(a) and 3(b) indicated that the exfoliated WS_2 had a lamellar structure with thin layers. Examples of few-layered sheets were observed for the processed WS_2 by SEM images shown in Figures 1(c), 3(c), and 3(d), which were smaller and much thinner than the bulk WS_2 presented in Figure 1(b). The lateral sizes of the processed sheets varied from 500 nm to 2 μm. The TEM and SEM images indicated that the WS_2 was successfully exfoliated into a few-layered nanostructure. As the uniform regular lattice was observed in the HR-TEM image in Figure 4, single crystal for WS_2 was shown clearly.

3.3. Thermal Analysis. The heat flow curves shown in Figure 5 and the thermogravimetric curves in Figure 6 corresponded to each other. The differential scanning calorimetry (DSC) curves had two decomposition peaks related to the primary decomposition and the secondary decomposition process, respectively, which was supported by literature [24, 25]. When the 1 wt% few-layered WS_2 was added, the initial decomposition temperature of the TKX-50 decreased by about 8.3°C, from 237.7 to 229.4°C. Upon adding the 1 wt% bulk WS_2, the decomposition temperature of the TKX-50 decreased by 7°C, from 237.7°C to 230.7°C. When the concentration of the WS_2 increased, its catalytic effect on the thermal decomposition of the TKX-50 increased. The initial decomposition temperatures of the TKX-50 were observed to be 13.1°C and 10.6°C depressed than the original ones, when the 3% few-layered and bulk samples were added. A

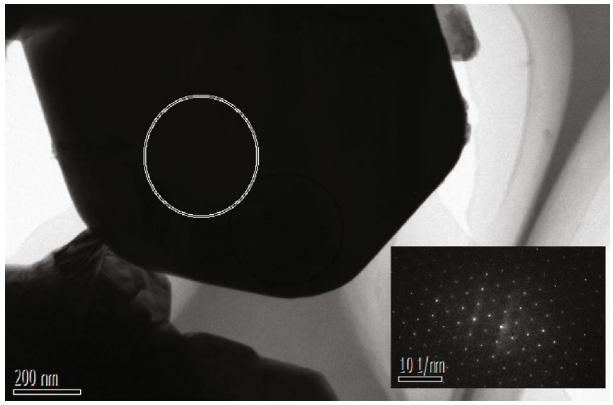

Figure 4: HR-TEM image of bulk WS_2.

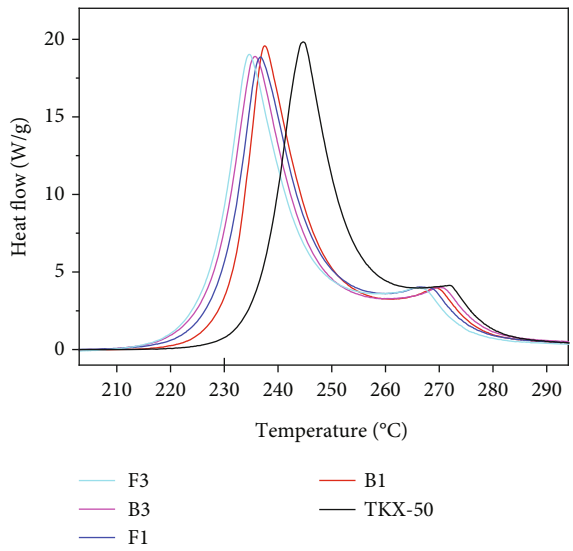

Figure 5: DSC curves of TKX-50, B1, F1, B3, and F3.

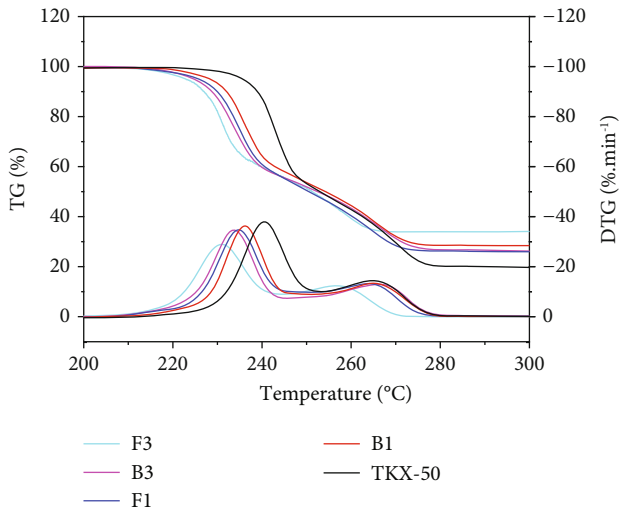

Figure 6: TG curves and DTG curves of TKX-50, B1, F1, B3, and F3 heating at 10 K·min^{-1}.

Table 2: The onset (T-onset) temperature and first (T-peak$_1$) and second peak temperatures (T-peak$_2$) of TKX-50, B1, F1, B3, and F3 in the DSC curves heating at 10 K·min^{-1}.

Sample	T-onset	T-peak$_1$	T-peak$_2$
TKX-50	237.7	243.7	271.9
B1	230.7	237.4	269.2
F1	229.4	236.8	261.7
B3	227.1	235.7	270.0
F3	224.6	234.7	257.1

Table 3: The first (T-peak$_1$) and second peak temperatures (T-peak$_2$) of TKX-50, B1, F1, B3, and F3 in the DTG curves heating at 10 K·min^{-1}.

Sample	T-peak$_1$	T-peak$_2$
TKX-50	240.5	265.1
B1	236.2	265.2
F1	234.8	263.7
B3	233.7	266.1
F3	231.0	256.7

summary of DSC results presented in Table 2 includes onset temperatures (T-onset) along with first (T-peak$_1$) and second peak temperatures (T-peak$_2$) for the TKX-50 containing different amounts of bulk and few-layered WS_2. The catalytic effects of the WS_2 were clearly observed as the T-onset, T-peak$_1$, and T-peak$_2$ decreased. Moreover, it was obvious that the WS_2 catalyst content (either bulk or few-layered) in the samples slightly decreased the peak height, as is shown in Figure 5.

TG curves and DTG curves presented in Figure 6 showed the thermogravimetry of the five samples. It could be seen from the figure that the addition of WS_2 led to the advance of the thermal weight loss of TKX-50 and the decrease of the weightlessness rate. The decrease of the weightlessness rate may be due to the fact that the added WS_2 will not decompose before 500°C. The advance TG and DTG mass loss curves give more evidence of the catalytic of WS_2 in the decomposition of TKX-50.

A possible mechanism proposed in this work could be verified through the DTG curves in Figure 6. The primary and secondary decompositions of TKX-50 were corresponding to two gas and energy release processes. The gas release could be reflected in the TG and DTG curves when the mass loss happened. The release of NH_3 and H_2O in the primary decomposition corresponded to the start temperatures and anterior peaks of DTG curves [26]. The release of CO_2, N_2, NH_3, N_2O, H_2O, etc. in the secondary decomposition related to the secondary peaks of DTG curves. Evidently, the addition of WS_2 led the initial temperature and primary maximum values of DTG curves ahead. A summary of the first (T-peak$_1$) and second peak temperatures (T-peak$_2$) of DTG curves is shown in Table 3. The T-peak$_1$ of B1 and B3 at 236.2°C and

233.7°C was higher than F1 and F3 at 234.8°C and 231.0°C and lower than the TKX-50 at 240.5°C, indicating that both two WS_2 could boost the primary decomposition of TKX-50 and few-layered WS_2 had a better catalytic effect. However, the secondary peak temperatures of DTG curves had no obvious change with the addition of WS_2, which could be concluded that the addition of WS_2 could boost the primary decomposition of TKX-50, but not the secondary one, and the few-layered WS_2 could be even more effective.

3.4. Thermokinetic Analysis. In order to compare the changes of E_a intuitively, two thermokinetic analytic procedures, the Kissinger method [27] (Equation (2)) and the Ozawa method [28] (Equation (3)) based on the Arrhenius equation (Equation (1)), were applied by using the AKTS software. AKTS uses the TG or DSC testing parameters to derive and evaluate the E_a without explicitly guessing a particular form of the reaction model $f(\alpha)$ [29].

$$\ln\left[\frac{\beta}{T_p^2}\right] = \ln\left[\frac{AR}{E}\right] - \frac{E}{RT_P}, \quad (1)$$

$$\lg\beta = \ln\frac{AE_a}{RF(\alpha)} - 2.315 - 0.4567\frac{E_a}{RT_p}, \quad (2)$$

$$\frac{d\alpha}{dt} = A\exp\left(-\frac{E}{RT(t)}\right)f(\alpha). \quad (3)$$

In these equations, α is the reaction progress, $f(\alpha)$ is the model function, A is the preexponential factor, E_a is the activation energy, t is the time, R is the ideal gas constant ($8.314\,J{\cdot}mol^{-1}{\cdot}K^{-1}$), and T is the absolute temperature.

The E_a analyzed by the Kissinger method was presented in Table 4. Upon analyzing the DSC curves, the E_a of the TKX-50 decreased from $159.867\,kJ{\cdot}mol^{-1}$ to 155.617 and $150.316\,kJ{\cdot}mol^{-1}$ after adding 1 wt% of raw and few-layered WS_2, respectively. Moreover, the E_a of the TKX-50 decreased more to 145.019 and $141.092\,kJ{\cdot}mol^{-1}$ after adding 3 wt% of bulk and few-layered WS_2, respectively. The changing trend of E_a calculated by the TG curve analysis, as is shown in Table 4, was consistent with that by the DSC curves. However, the values were slightly different. After the addition of 1 wt% of raw and few-layered WS_2, the E_a of the TKX-50 decreased from $169.66\,kJ{\cdot}mol^{-1}$ to 154.946 and $145.316\,kJ{\cdot}mol^{-1}$, respectively. Upon adding 3 wt% bulk and few-layered WS_2, the E_a of the TKX-50 decreased to $141.271\,kJ{\cdot}mol^{-1}$ and $137.837\,kJ{\cdot}mol^{-1}$ which indicated the better catalysis of few-layered WS_2.

The E_a calculated by the Kissinger method indicated that both raw and treated WS_2 could reduce the E_a of TKX-50 thermal decomposition, and the few-layered WS_2 could abate it more. Moreover, increasing the catalyst content in the material could enhance its catalytic effect.

The E_a calculated by the Ozawa method were consistent with the Kissinger method. As shown in Figure 7(a), during the reaction progress from 0.1 to 0.9, the E_a decreased with the 1 wt% addition of the WS_2, which demonstrated the catalysis of bulk and few-layered WS_2. Besides, F1 and F3 had the lower E_a than B1 and F3 in Figures 7(a) and 7(b). The E_a curves in Figures 7(a) and 7(b) shared similar data trends, which indicated that these five samples likely followed the same reaction mechanism.

The E_a calculated with the TG curves using the Ozawa method in Figures 7(c) and 7(d) showed similar trends with above results, though the relevancy of the E_a curve obtained by the analysis of the TG curve was not as good as that of the DSC curves.

The result of thermal and thermokinetic analysis could be concluded as follows. Compared with the pure TKX-50, the addition of few-layered and bulk WS_2 promoted its thermal decomposition. The sample in the absence of the WS_2 catalyst had the highest initial decomposition temperature and E_a, while the sample containing 3 wt% of the few-layered catalyst had the lowest initial decomposition temperature and E_a. The increase in the concentration of the WS_2 further promoted thermal decomposition, and the few-layered catalyst enhanced the decomposition of the TKX-50 more compared to the bulk one.

As was seen in Figure 8, a possible mechanism was proposed that WS_2 materials were excited when the heating energy was greater than the band gap energy and then electron-hole pairs separated [30]. Separated conduction-band electrons and valence band holes would cause fast charge transfer and promote the proton transfer from H atom of NH_3OH^+ to O atom of bisteterazole in the TKX-50 [31]. NH_3OH^+ is not stable in high temperature and would decompose into NH_3 and H_2O with energy release. With more surface area, more active sites, more exposed edges, and better electrical conductivity, few-layered WS_2 would increase the proton transfer activity than the raw material. Furthermore, supported by the DTG and DSC curves, the existence of WS_2 promoted the decomposition and recombination of NH_3OH^+ with producing H_2O and NH_3 which caused gas and initial energy release to advance.

4. Conclusion

In summary, a novel and effective few-layered catalyst for the energetic salt TKX-50 was prepared. A thermal analysis of the TKX-50 mixed with different ratios of bulk and few-layered WS_2 was carried out to study the effects of bulk and few-layered WS_2 on the thermal decomposition of TKX-50. The results are concluded as follows:

(i) Raw WS_2 tablets were peeled off using the LPE method, and few-layered sheets were found in the exfoliated samples.

(ii) Both bulk WS_2 and processed few-layered WS_2 could promote the decomposition of TKX-50 and reduced its activation energy; at the same time, the few-layered WS_2 had a better catalytic effect because it exposed more active sites.

(iii) A possible mechanism was proposed: the WS_2 catalyzed thermal decomposition of the TKX-50 because the WS_2 improved the ability of proton

Table 4: The value of activation energy calculated by the Kissinger method.

Sample	TKX-50	B1	F1	B3	F3
E_a by DSC curves (kJ·mol^{-1})	159.867	155.617	150.316	145.019	141.092
E_a by TG curves (kJ·mol^{-1})	169.66	154.946	145.316	141.271	137.837

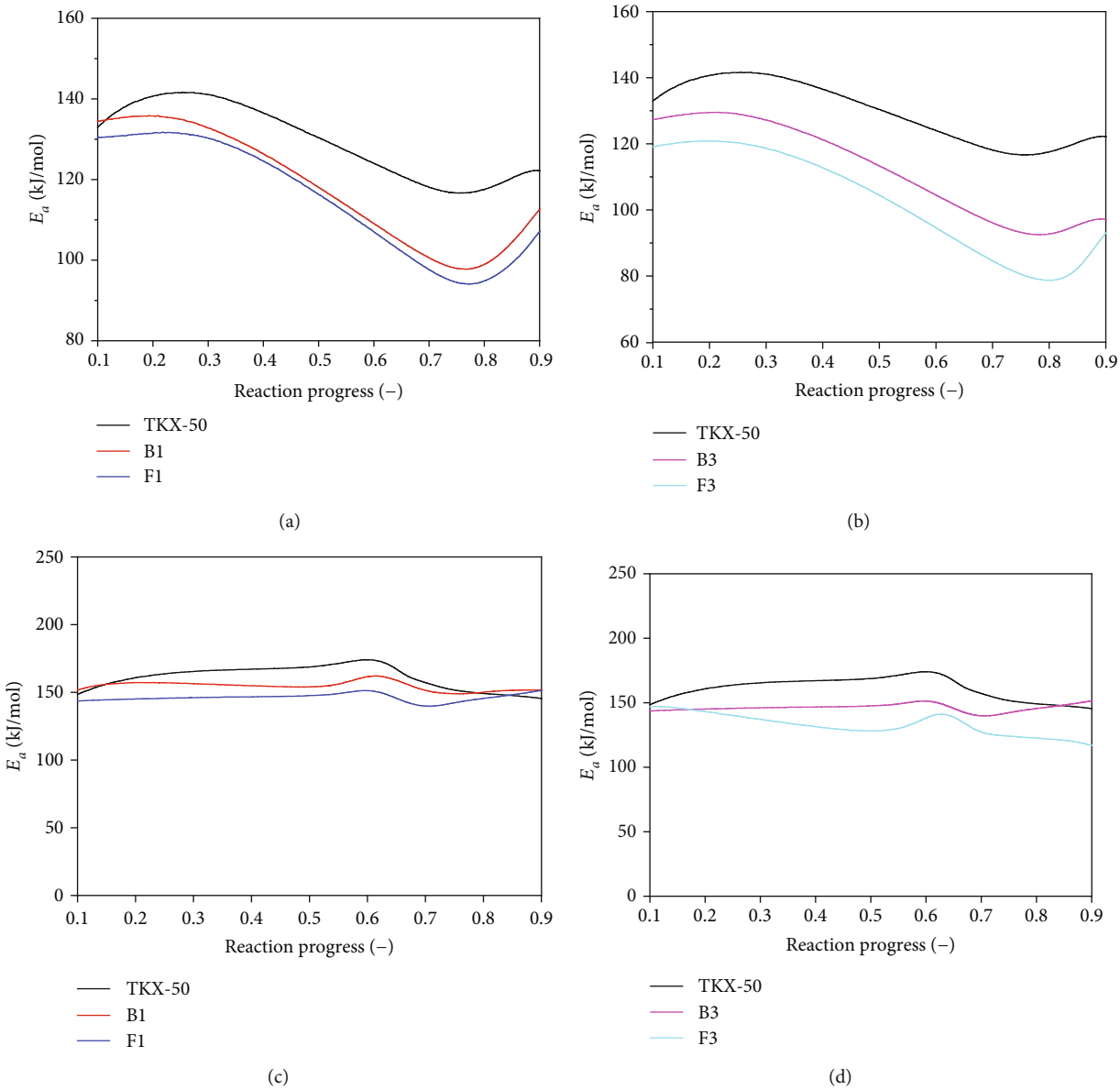

Figure 7: (a) E_a of TKX-50, B1, and F1 calculated by DSC curves through the Ozawa method. (b) E_a of TKX-50, B3, and F3 calculated by DSC curves through the Ozawa method. (c) E_a of TKX-50, B1, and F1 calculated by TG curves through the Ozawa method. (d) E_a of TKX-50, B3, and F3 calculated by TG curves through the Ozawa method.

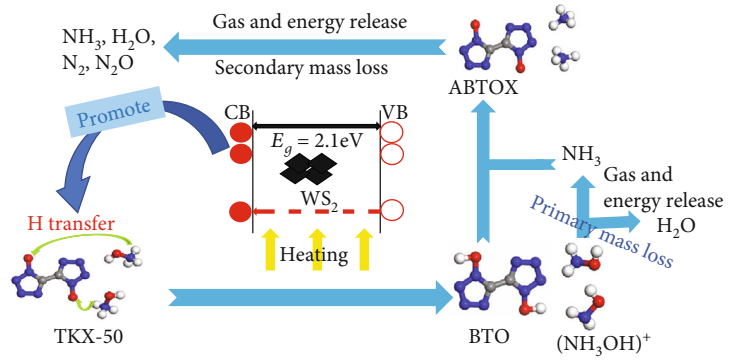

Figure 8: Schematic diagram of the thermal decomposition with WS_2.

transfer and promoted the initiation of the TKX-50 decomposition. The exposed active surface of the WS_2 few-layered sheets can be more effective in facilitating the decomposition of the TKX-50 for its stronger ability to promote proton transfer, indicating that the LPE method is a promising approach to improve the catalytic performance of WS_2

Data Availability

The (data type) data used to support the findings of this study are included within the article.

Conflicts of Interest

The authors declare that they have no conflicts of interest.

References

[1] N. Fischer, D. Fischer, T. M. Klapötke, D. G. Piercey, and J. Stierstorfer, "Pushing the limits of energetic materials – the synthesis and characterization of dihydroxylammonium 5,5′-bistetrazole-1,1′-diolate," *Journal of Materials Chemistry*, vol. 22, no. 38, article 20418, 2012.

[2] X. Cao, Y. Shang, K. Meng et al., "Fabrication of three-dimensional TKX-50 network-like nanostructures by liquid nitrogen-assisted spray freeze drying method," *Journal of Energetic Materials*, vol. 37, no. 3, pp. 356–364, 2019.

[3] P. Deng, J. Xu, S. Li et al., "A facile one-pot synthesis of monodisperse hollow hexanitrostilbene-piperazine compound microspheres," *Materials Letters*, vol. 214, pp. 45–49, 2018.

[4] P. Deng, H. Ren, and Q. J. Jiao, "Enhanced thermal decomposition performance of sodium perchlorate by molecular assembly strategy," *IONICS*, pp. 1–6, 2019.

[5] X. Cao, P. Deng, S. Hu et al., "Synthesis and characterization of energetic hollow spherical hexanitro-stilbene derivatives," *Nanomaterials*, vol. 6, no. 5, p. 336, 2018.

[6] P. Deng, Y. Liu, P. Luo et al., "Two-steps synthesis of sandwich-like graphene oxide/LLM-105 nanoenergetic composites using functionalized graphene," *Materials Letters*, vol. 194, pp. 156–159, 2017.

[7] P. Deng, H. Ren, and Q. Jiao, "Enhanced the combustion performances of ammonium perchlorate-based energetic molecular perovskite using functionalized graphene," *Vacuum*, vol. 169, article 108882, 2019.

[8] W. Chen, L. Chang, S.-B. Ren, Z.-C. He, G.-B. Huang, and X.-H. Liu, "Direct Z-scheme 1D/2D $WO_{2.72}/ZnIn_2S_4$ hybrid photocatalysts with highly-efficient visible-light-driven photodegradation towards tetracycline hydrochloride removal," *Journal of Hazardous Materials*, vol. 384, article 121308, 2020.

[9] S. Ahmed and J. Yi, "Two-dimensional transition metal dichalcogenides and their charge carrier mobilities in field-effect transistors," *Nano-Micro Letters*, vol. 9, no. 4, p. 50, 2017.

[10] W. Ho, J. C. Yu, J. Lin, J. Yu, and P. Li, "Preparation and photocatalytic behavior of MoS_2 and WS_2 nanocluster sensitized TiO_2," *Langmuir*, vol. 20, no. 14, pp. 5865–5869, 2004.

[11] A. L. Elias, C. Janisch, A. Cocking et al., "Synthesis and integration of TMDs into nonlinear optical devices," APS Meeting Abstracts, 2017.

[12] P. Joensen, R. F. Frindt, and S. R. Morrison, "Single-layer MoS_2," *Materials Research Bulletin*, vol. 21, no. 4, pp. 457–461, 1986.

[13] K. S. Novoselov, D. Jiang, F. Schedin et al., "Two-dimensional atomic crystals," *Proceedings of the National Academy of Sciences*, vol. 102, no. 30, pp. 10451–10453, 2005.

[14] A. Splendiani, L. Sun, Y. Zhang et al., "Emerging photoluminescence in monolayer MoS_2," *Nano Letters*, vol. 10, no. 4, pp. 1271–1275, 2010.

[15] J. N. Coleman, M. Lotya, A. O'Neill et al., "Two-dimensional nanosheets produced by liquid exfoliation of layered materials," *Science*, vol. 331, no. 6017, pp. 568–571, 2011.

[16] A. Ambrosi, Z. Sofer, and M. Pumera, "2H → 1T phase transition and hydrogen evolution activity of MoS_2, $MoSe_2$, WS_2 and WSe_2 strongly depends on the MX_2 composition," *Chemical Communications*, vol. 51, no. 40, pp. 8450–8453, 2015.

[17] C. Tan and H. Zhang, "Two-dimensional transition metal dichalcogenide nanosheet-based composites," *Chemical Society Reviews*, vol. 44, no. 9, pp. 2713–2731, 2015.

[18] H. Zhao, H. Wu, J. Wu et al., "Preparation of MoS_2/WS_2 nanosheets by liquid phase exfoliation with assistance of epigallocatechin gallate and study as an additive for high-performance lithium-sulfur batteries," *Journal of Colloid and Interface Science*, vol. 552, pp. 554–562, 2019.

[19] V. Zatko, M. Galbiati, S. M. M. Dubois et al., "Band-structure spin-filtering in vertical spin valves based on chemical vapor deposited WS_2," *ACS Nano*, 2019.

[20] D. Voiry, H. Yamaguchi, J. Li et al., "Enhanced catalytic activity in strained chemically exfoliated WS_2 nanosheets for hydrogen evolution," *Nature Materials*, vol. 12, no. 9, pp. 850–855, 2013.

[21] Q. Lu, Y. Yu, Q. Ma, B. Chen, and H. Zhang, "2D transition-metal-dichalcogenide-nanosheet-based composites for photocatalytic and electrocatalytic hydrogen evolution reactions," *Advanced Materials*, vol. 28, no. 10, pp. 1917–1933, 2016.

[22] J. Zhang, S. Liu, H. Liang, R. Dong, and X. Feng, "Hierarchical transition-metal dichalcogenide nanosheets for enhanced electrocatalytic hydrogen evolution," *Advanced Materials*, vol. 27, no. 45, pp. 7426–7431, 2015.

[23] J. Shen, Y. He, J. Wu et al., "Liquid phase exfoliation of two-dimensional materials by directly probing and matching surface tension components," *Nano Letters*, vol. 15, no. 8, pp. 5449–5454, 2015.

[24] N. V. Muravyev, K. A. Monogarov, A. F. Asachenko et al., "Pursuing reliable thermal analysis techniques for energetic materials: decomposition kinetics and thermal stability of dihydroxylammonium 5,5′-bistetrazole-1,1′-diolate (TKX-50)," *Physical Chemistry Chemical Physics*, vol. 19, no. 1, pp. 436–449, 2017.

[25] P. Wang, Q. Xie, Y. G. Xu, J. Q. Wang, Q. H. Lin, and M. Lu, "A kinetic investigation of thermal decomposition of 1,1′-dihydroxy-5,5′-bitetrazole-based metal salts," *Journal of Thermal Analysis and Calorimetry*, vol. 130, no. 2, pp. 1213–1220, 2017.

[26] Q. An, W. G. Liu, W. A. Goddard III, T. Cheng, S. V. Zybin, and H. Xiao, "Initial steps of thermal decomposition of dihydroxylammonium 5,5′-bistetrazole-1,1′-diolate crystals from quantum mechanics," *The Journal of Physical Chemistry C*, vol. 118, no. 46, pp. 27175–27181, 2014.

[27] H. E. Kissinger, "Variation of peak temperature with heating rate in differential thermal analysis," *Journal of Research of the National Bureau of Standards*, vol. 57, no. 4, p. 217, 1956.

[28] T. Ozawa, "A new method of analyzing thermogravimetric data," *Bulletin of the Chemical Society of Japan*, vol. 38, no. 11, pp. 1881–1886, 1965.

[29] H.-M. Zou, S.-S. Chen, X. Li et al., "Preparation, thermal investigation and detonation properties of ε-CL-20-based polymer-bonded explosives with high energy and reduced sensitivity," *Materials Express*, vol. 7, no. 3, pp. 199–208, 2017.

[30] L. Su, Y. Yu, L. Cao, and Y. Zhang, "Effects of substrate type and material-substrate bonding on high-temperature behavior of monolayer WS_2," *Nano Research*, vol. 8, no. 8, pp. 2686–2697, 2015.

[31] J. Jia, Y. Liu, S. Huang et al., "Crystal structure transformation and step-by-step thermal decomposition behavior of dihydroxylammonium 5,5′-bistetrazole-1,1′-diolate," *RSC Advances*, vol. 7, no. 77, pp. 49105–49113, 2017.